RSC Advances

ROYAL SOCIETY OF CHEMISTRY

www.rsc.org/advances

RSC Advances

ARTICLE

Remote Triggering of Thermoresponsive PNIPAM by Iron Oxide Nanoparticles

Received 00th October 2015,
Accepted 00th December 2015

DOI: 10.1039/x0xx00000x

www.rsc.org/

D. J. Denmark,[a,†] J. Bradley,[a,b] D. Mukherjee,[a] J. Alonso,[a,c] S. Shakespeare,[a] N. Bernal,[a] M. H. Phan,[a] H. Srikanth,[a] S. Witanachchi,[a] and P. Mukherjee[a]

A thorough study on the elements that affect the lower critical solution temperature (LCST) of poly(N-isopropylacrylamide) (PNIPAM) solutions during alternating magnetic field (AMF) heating, using iron oxide magnetic nanoparticles (IO MNPs) is reported. Several PNIPAM solutions with different concentrations of IO MNPs were prepared and characterized using transmission electron microscopy, dynamic light scattering, and Raman spectroscopy. While increasing the IO MNP concentration was observed to decrease the specific absorption rate (SAR), the presence of PNIPAM in the solution facilitated the dispersal and disaggregation of IO MNPs leading to a slight improvement in the SAR. In-situ transmission measurements were used to determine the LCST of PNIPAM under various aqueous concentrations with dispersed IO MNPs. A systematic decrease in the LCST from 34 °C to 31 °C was observed as the concentration of PNIPAM was increased from 0.3 wt. % to 1.0 wt. %, while keeping the concentration of IO MNPs constant. On the other hand, varying the ion concentration of the PNIPAM solutions by adding adjusted KOH pellets, showed a pronounced lowering of the LCST by 3-4 °C at all PNIPAM concentrations, which has been shown to be further affected by the presence of the nanoparticles. The remote triggering of volume phase transition in PNIPAM solutions by raising the temperature above the LCST using IO MNPs as reported here is important in targeted drug-delivery applications using thermo-responsive polymers.

Introduction

In recent years there has been a surge of interest in the use of multifunctional nanocarriers for improving the efficiency of different biomedical applications [1-12]. When properly engineered, these multifunctional nanocarriers, besides carrying the therapeutic agent (e.g. drugs, genes, donor cells, etc.), can demonstrate a combination of various advantageous properties/functions [2,10]. More specifically, in the field of drug delivery, nanotechnologists combine the carrying capability and stimuli-responsive nature of certain hydrogels with the properties of magnetic nanoparticles (MNPs) to obtain a product that gives both targeted and remote delivery of therapeutic agents. The targeted delivery aspect of the product comes from the force of attraction felt by the MNPs in a static magnetic field, and remote delivery aspect of the product is a consequence of the temperature increase in the vicinity of the MNPs when exposed to an alternating magnetic field (AMF) [13,14]. This temperature increase then leads to a volume phase transition (VPT) of the thermoresponsive polymer prompting it to release the therapeutic payload [1,4].

Thermoresponsive hydrogels such as poly(N-isopropylacrylamide) (PNIPAM) exhibit reversible shrinking or swelling when heated; this makes them attractive candidates for a wide range of controlled release applications like drug delivery and oil separation [15-19]. Biocompatible PNIPAM has a lower critical solution temperature (LCST) of approximately 32 °C due to the presence of both hydrophilic amide and hydrophobic isopropyl and acrylic groups in its monomer structure, NIPAM. Below the LCST, enthalpy dominated PNIPAM is in its hydrophilic conformation and disperses easily in water. However, as the temperature increases the hydrogen bonds responsible for PNIPAM's stability in solution weaken and, above the LCST, PNIPAM precipitates (shrinks) out of solution, being dominated now by entropy [20]. This VPT manifests as an increase in the turbidity of the solution above the LCST (cloud point temperature). The triggering of VPT in PNIPAM is sensitive to changes in the polymer concentration (as long as the concentration is beneath the critical micelle concentration) and the pH (via addition of NaCl, KOH, etc.) of the solution [21,22].

Practical applications such as drug delivery require remote triggering of PNIPAM hydrogels which can be realized by the heating of magnetic nanoparticles (MNPs) (dispersed in the hydrogel solutions) by exposing them to external radio-frequency (RF), alternating magnetic field (AMF). Typically, the heat generated by MNPs is related to hysteresis losses which are proportional to the magnetic hysteresis loop area described by the magnetic moments of the nanoparticles when exposed to the AMF [23]. Heat generation using biocompatible IO MNPs has been widely studied for efficient magnetic heating (temperature range 40-45 °C) in hyperthermia applications due to their desirable magnetic and inductive heating properties

[a] Department of Physics, University of South Florida, Tampa, FL 33620
[b] Department of Bioengineering, University of Missouri, Columbia, MO 65211
[c] BCMaterials Edificio Nº. 500, Parque Tecnológico de Vizcaya, Derio, Spain 48160
† Corresponding Author: denmark@mail.usf.edu

[24-27]. In contrast to the hyperthermia applications where heat damage is initiated by exposing diseased tissue to elevated temperatures for a period of time, drug delivery applications using MNPs embedded in thermo-responsive polymers require controlled heating (temperature change of 4-10 °C) in short time intervals. This is particularly challenging since any excessive heating of the polymer (PNIPAM) can degrade its structural integrity and consequently destroy its reversible VPT behavior.

For most biological applications, it is considered that the suitable size of the IO MNPs should be less than 100 nm [28]. The optimal size is further reduced when considering that larger particles in this range tend to aggregate potentially causing emboli and that they have shorter half-lives in the blood stream due to a triggering of the immune response [29]. Considering this, the use of non-aggregating superparamagnetic IO MNPs (SPIONs) has been favored for biomedical applications [28-30]. Superparamagnetic behavior can be inferred from RT hysteresis loops with a Langevin-like shape showing that there is no coercivity or remanence. For SPIONs, the heat generation under RF fields is primarily attributed to susceptibility losses [23,31]. The magnetic moments of IO MNPs spontaneously reverse direction under the influence of an AMF and in the process transfer the heat energy to the surrounding environment.

At the time of this writing, the field is somewhat deficient in studies that systematically investigate the VPT of linear PNIPAM when heated by MNPs responding to an AMF. There has been, for example, a study by Zadrazil et. al, in which the release of entrapped oil from PNIPAM hydrogels in response to AMF heating was observed [32]. Similarly, Cejková et. al demonstrated the release of vitamin B12 from PNIPAM microdroplets [33]. However, a pure examination of PNIPAM's VPT in response to AMF heating is missing in these studies, and an emerging important question is how the heating efficiency of MNPs would change once the MNPs are embedded in PNIPAM. Such knowledge is essential to tailor the dual functional response of MNP-embedded PNIPAM composites for a wide range of biomedical applications, including targeted drug delivery.

To address these important issues, we have performed a thorough study on the evolution of the LCST of PNIPAM loaded with SPIONs in response to the remotely triggered heating by a variable AMF. We have analysed the evolution of the LCST as a function of both the polymer and the nanoparticle concentration, and we have also examined the effect of the different ion concentration (ph modification) on the thermal response of PNIPAM.

Materials and methods

Aqueous solutions were prepared by mixing desired amounts of high purity PNIPAM (99.9 %, mol. wt. 10,000 g/mol, Sigma Aldrich) powder and commercial chemically synthesized IO MNPs with PVP coating (99.5 % pure, US Research Nanomaterials, Inc.) in deionized water (DIW) or water that had adjusted KOH dissolved therein at a 0.10 M concentration. Transmission electron microscopy (TEM) of the MNPs dispersed in hexane and drop cast onto Cu grids was carried out with a FEI Morgani system operated at 60 kV acceleration voltage. The MNPs were homogeneously dispersed in the solutions by repeated ultrasonication in ice-bath (to avoid any extrinsic heating). Raman spectra of the prepared solutions (before and after heating) were acquired using a Horiba Jobin Yvon T64000 Advanced Research Raman System equipped with an argon laser operated at 514 nm. Dynamic light scattering (DLS) measurements were carried out using a Malvern Instruments Zetasizer Nano S model ZEN1600 operating at 632.8 nm. Solutions studied by DLS were dispersed in a polystyrene cuvette.

For transmission measurements, 2.0 mL of the dispersed solution was transferred to a polystyrene optical cuvette that was suspended in the RF heating coil. The turbidity change of solution associated with the VPTs in the PNIPAM/IO MNP solutions was detected using a home-made setup (see Fig. 1). Transmission measurements were carried out with a 25 mW He-Ne laser (CW Radiation, Inc.) of 633 nm wavelength. The laser was aligned so as to pass between the loops of the coil and through the optical cuvette as shown in Fig. 1. The transmitted laser beam was incident on a cadmium-sulfide photodetector and the change in resistance was measured as a function of time using a Keithley 2100 Multimeter and LabView programmed for data acquisition. The PNIPAM/IO MNP solutions, within the cuvette, were heated using an AMF at an optimum amplitude of 740 Oe using an Ambrell EasyHeat LI heating system operating at a frequency of 307 kHz. The photodetector and RF heating coil are separated by more than 10 cm so that the effect of the AC magnetic field on the photodetector is negligible. The temperature evolution of a given solution was measured as a function of time. Temperature changes in the solution, induced by the RF heating system, were monitored by an optical temperature sensor (Photon Control) with an accuracy of +/- 0.05°C.

Generally, in hyperthermia experiments, there are two sources of heat generated in a sample. What is of interest is the heat generated by the MNPs as a result of their exposure to the AMF. However, systems like the one used in this work employ water cooling of the RF heating coil to reduce the unintentional heating of the sample due to convective heating from the coil. Despite this measure there is still some unintentional heating of the sample that must be corrected for. One established method for calibrating data involves running control trials involving samples of the solvent only and subtracting that heating curve from that of the sample that includes both the solvent and the MNPs [34]. This method, however, is insufficient for the experiments discussed herein. Samples containing PNIPAM are necessarily influenced by the convective heat generated by the RF heating coil. That effect cannot be corrected for mathematically; it must be physically removed from the experimental system. The setup, therefore, was augmented by the addition of a fan beneath the RF heating coil to supply it with a continuous flow of air which provided additional removal

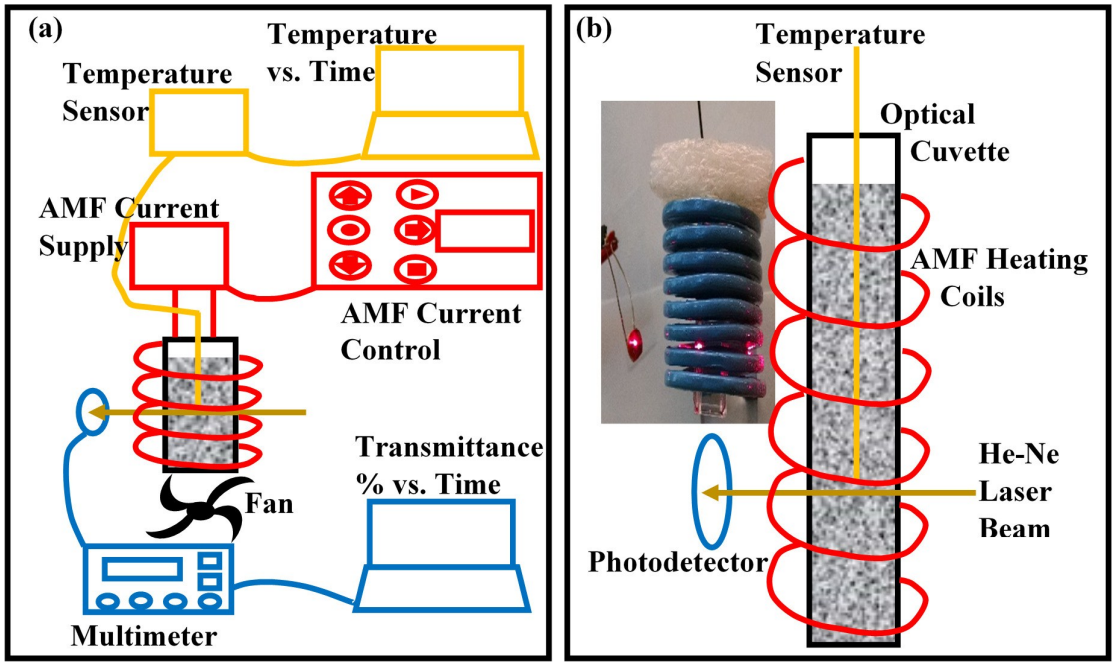

Fig. 1 (a) In this custom-built experimental setup, the turbidity of a solution as a function of time can be probed and synchronized with the solution's temperature as a function of time, all while the solution, containing PNIPAM and IO MNPs dispersed in DIW, is subject to an AMF. (b) Note that the He-Ne laser, seen in the inset photograph passing through the AMF heating coils and cuvette to land on the photodetector, probes the solution in proximity to the placement of the temperature sensor so as to ensure the turbidity data correlates to the temperature data.

of heat from the coil (see Fig. 1). This gave an effective zero slope heating curve when measuring the water background.

Results and Discussion

Characterization of PNIPAM and IO MNP.

The size and morphology of IO MNPs was investigated by TEM. The commercially purchased MNPs are shown in Fig. 2(a) and 2(b). As can be seen, they are polydisperse and non-uniform in shape with an average size of 9.9 ± 1.4 nm. When IO MNPs are dispersed in DIW alone they tend to form relatively large aggregates as can be seen in Fig. 2(a). On the other hand, by dispersing the same concentration of IO MNPs in DIW that also contains PNIPAM significantly smaller aggregates are generally observed, as shown in Fig. 2(b). The ability of PNIPAM to facilitate the dispersal and disaggregation of IO MNPs in solution is further demonstrated by Fig. 2(c). Here DLS is provided to compare the hydrodynamic size of IO MNP aggregates. When IO MNPs are dispersed alone in DIW (black curve) there are two relatively large populations of aggregates. The larger, more prominent population of aggregates has an average hydrodynamic diameter of 770 ± 167 nm, while the smaller, less prominent population of aggregates is 229 ± 41 nm in size. Now when PNIPAM is present in solution the two populations of IO MNP aggregates are significantly smaller: 356 ± 54 nm and 75 ± 9 nm, respectively. Clearly the presence of PNIPAM effectively reduces the size of IO MNP aggregates.

In Fig. 2(d) the magnetization as a function of applied magnetic field is plotted, recorded at room temperature. No coercivity or remanence is observed suggesting that the nanoparticles exhibit a superparamagnetic-like behavior at room temperature. To confirm this, we fit our hysteresis loops to a standard Langevin expression:

$$M(H)=M_S \int_0^\infty L\left(\frac{\mu H}{k_B T}\right) f(D)dD \qquad (1)$$

where D is the diameter of the nanoparticles, f(D) corresponds with a Log-Normal size distribution, and L(x) = cotanh(x)-1/x. As seen from Fig. 2(d), the fitting result is very good, although the apparent size obtained from this fit is a little bit smaller than expected, 7.8 nm. This is likely due to the effect of surface spin disorder which effectively reduces the apparent magnetic size of the nanoparticles. Surface spin disorder is also believed to result in a significantly reduced total magnetization of our MNPs (MS ~60 emu/g) relative to bulk Fe_3O_4 (MS ~90 emu/g).

The Raman spectrum of the samples was recorded, and is shown in Fig. 3(a), both before and after ten heating trials to confirm that the PNIPAM was not damaged after several

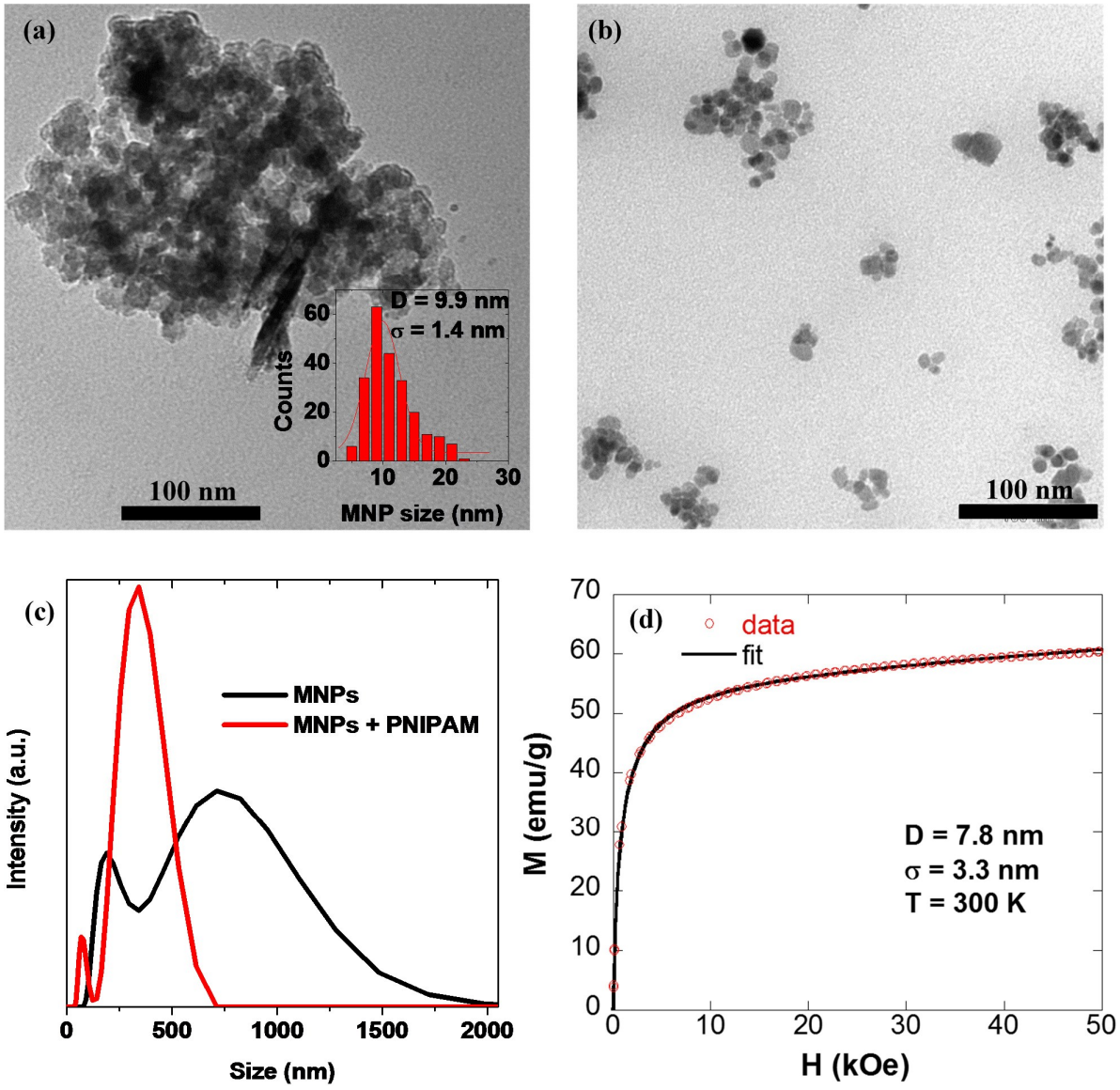

Fig. 2 (a) TEM of IO MNPs showing large aggregates when PNIPAM is not present. The IO MNP size distribution is plotted in the inset. (b) TEM of IO MNPs showing relatively smaller aggregates when PNIPAM is not present. Note that for both (a) and (b) the IO MNP concentration is the same. (c) Hydrodynamic size distributions are given by DLS measurements of a solution containing MNPs only in DIW (black curve) and a solution containing MNPs dispersed in DIW in which PNIPAM is present (red curve). The concentration of IO MNPs is the same in both solutions. (d) Magnetization data obtained at 300 K reveals the superparamagnetic nature of the IO MNPs and an average size of 7.8 ± 3.3 nm.

heating/cooling cycles and to establish that the phase change is reversible. Peaks like the one at 1459 cm^{-1} are indicative of the hydrophobic isopropyl part of the monomer while the ones like the peak at 1645 cm^{-1} indicate the hydrophilic amide part of the monomer. The peaks at 3297 cm^{-1} and 3440 cm^{-1} indicate the water is H-bonded to the oxygen atom on the amide. The three most prominent peaks around 2925 cm^{-1} are instructive of the hygroscopic nature of PNIPAM [36].

Finally, in Figs. 3(b-d) a series of photographs is presented to document the appearance of the solutions discussed in the following sections. When the temperature of PNIPAM is less than the LCST the Gibbs free energy is enthalpy dominated, H-bonding between the DIW and amide section is stable allowing the polymer to dissolve in solvent, and the sample appears clear like the left image in Fig. 3(b). On the other hand, if the temperature of PNIPAM rises above the LCST, then the entropy dominated Gibbs free energy leads to disruption of the H-bonding so that the polymer precipitates out of solution, which causes the sample to appear turbid like the right image in Fig. 3(b). Now when IO MNPs are present, the solution becomes darker as their concentration increases, as is demonstrated in

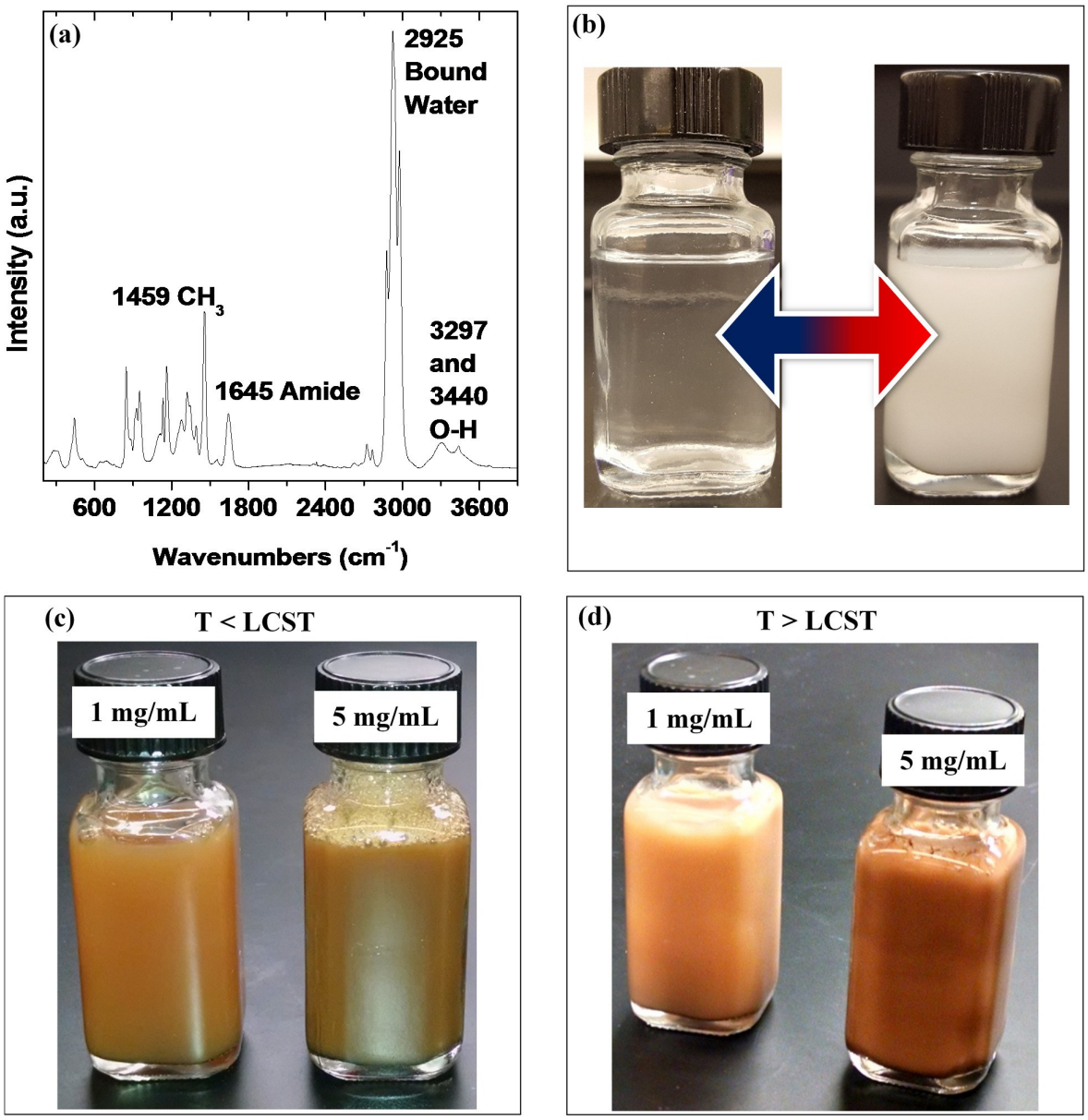

Fig. 3 (a) Raman spectroscopy of PNIPAM after being subjected to 10 trials of AMF heating reveal the polymer was undamaged during the trials. (b) A 1.0 wt. % aqueous solution of PNIPAM below the LCST appears clear, while the same solution appears turbid when it is heated above its LCST. (c) By increasing the IO MNP concentration the solution's color darkens. (d) By increasing the temperature of the same solutions in (c) the sample takes on a white/milky quality indicating the PNIPAM has precipitated out of the solution.

Fig. 3(c). When those same solutions were heated to a temperature above the LCST, the polymer precipitates as indicated by white/milky quality of the samples in Fig. 3(d).

3.2. AMF Heating with IO MNPs

Preliminary AMF heating experiments focused on finding the optimum IO MNP concentrations to use in the transmittance experiments discussed in the next two sections. Five samples were prepared in optical cuvette, as described above, with differing IO MNP to DIW mass so that the concentrations investigated ranged from 1 to 5 mg/mL. The change in temperature as a function of time for each of these five concentrations is given in Fig. 4(a). The average of ten trials

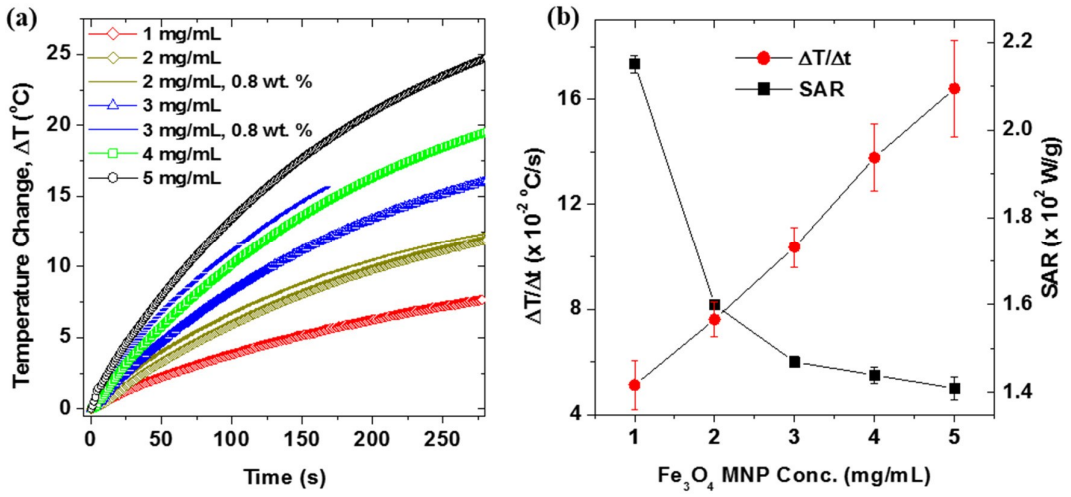

Fig. 4 (a) Heating curves of solutions containing IO MNPs dispersed in DIW at concentrations ranging from 1 to 5 mg/mL. Also shown, are the heating curves for a 2 and 3 mg/mL solution that also contains 0.8 wt. % PNIPAM. (b) A comparison of initial linear heating rates and SARs as a function of IO MNP concentration.

for each sample is given here. As expected, the higher the concentration of MNPs in solution the more effective the heating of the entire sample is. For example, at 1 mg/mL the solution in cuvette experienced a nearly 7.5 °C temperature increase after being exposed to an AMF for 280 s. At the other end of the IO MNP concentration range, at 5 mg/mL the sample increased nearly 25 °C under the same AMF conditions. However, this data only reports on the global heating of the sample.

In order to comment on the heating efficiency of the nanoparticles one must calculate the specific absorption rate (SAR) which is given by

$$SAR = \frac{c_{sol} m_{sol}}{m_{MNP}} \left(\frac{\Delta T}{\Delta t}\right) \qquad (2)$$

where c_{sol} is the specific heat of the solution, m_{sol} the mass of the solution, m_{MNP} the mass of the nanoparticles, and $\Delta T/\Delta t$ the initial slope of the heating curves. The initial, linear slope of the heating curve and SAR of all five concentrations is plotted as a function of IO MNP concentration in Fig. 4(b). Again, the initial heating rates of the entire sample increases as IO MNP concentration increases. Nevertheless, the SAR decreases with increasing IO MNP concentration. This reduction in the heating efficiency with increasing concentration has been consistently reported in the literature [37] and attributed to the higher aggregation of the nanostructures as their concentration increases, which tends to negatively affect their heating capacity. Considering these results, it was decided to focus on the concentration around the crossover region of Fig. 4(b), 2 mg/mL, for the experiments discussed below. Selecting 2 mg/mL allows for effective heating of the local environment and relatively slow heating of the sample. In addition, we have also studied the results for the samples with 3 mg/mL IO MNP concentration, which provides for relatively fast heating of the sample, but reduced efficacy of local environment heating, in order to see the differences with respect to 2 mg/mL.

One question that could be raised is how the heating efficiency of the nanoparticles would change once they are embedded in PNIPAM instead of just DIW. To shed light on this, we have measured the heating curves, Fig. 4(a), for samples that contained both IO MNPs and 0.8 wt. % PNIPAM in solution with DIW. Both of these samples showed increased heating rates as compared to their corresponding sample that had no PNIPAM within it. This can be related to the fact that the presence of PNIPAM in solution facilitates the dispersal and disaggregation of the IO MNPs, as was shown before by TEM and DLS measurements (see Fig. 2). It has been shown in the literature that particle aggregation can profoundly affect SAR values, and often in a detrimental way, due to the enhancement of the dipolar interactions [38]. In our case, the disaggregation leads to a slightly improved heating efficacy for MNPs when embedded in PNIPAM. Interestingly, for a 3 mg/mL IO MNP solution that also contains PNIPAM the increase in heating efficiency, compared with the same concentration solution without PNIPAM, is more dramatic than for a 2 mg/mL solution with PNIPAM, as shown in Fig. 4(a).

3.3. Probing the LCST of PNIPAM heated with AMF

Figures 5(a) and 5(b) show the temperature-dependent transmission characteristics at wavelength of 633 nm obtained for two aqueous solutions of PNIPAM with 2 mg/mL and 3 mg/mL of MNPs at various polymer concentrations ranging from 0.3 to 1.0 wt. %. From the data it is evident that the inflection point where the transmittance drops from 100 % to 0

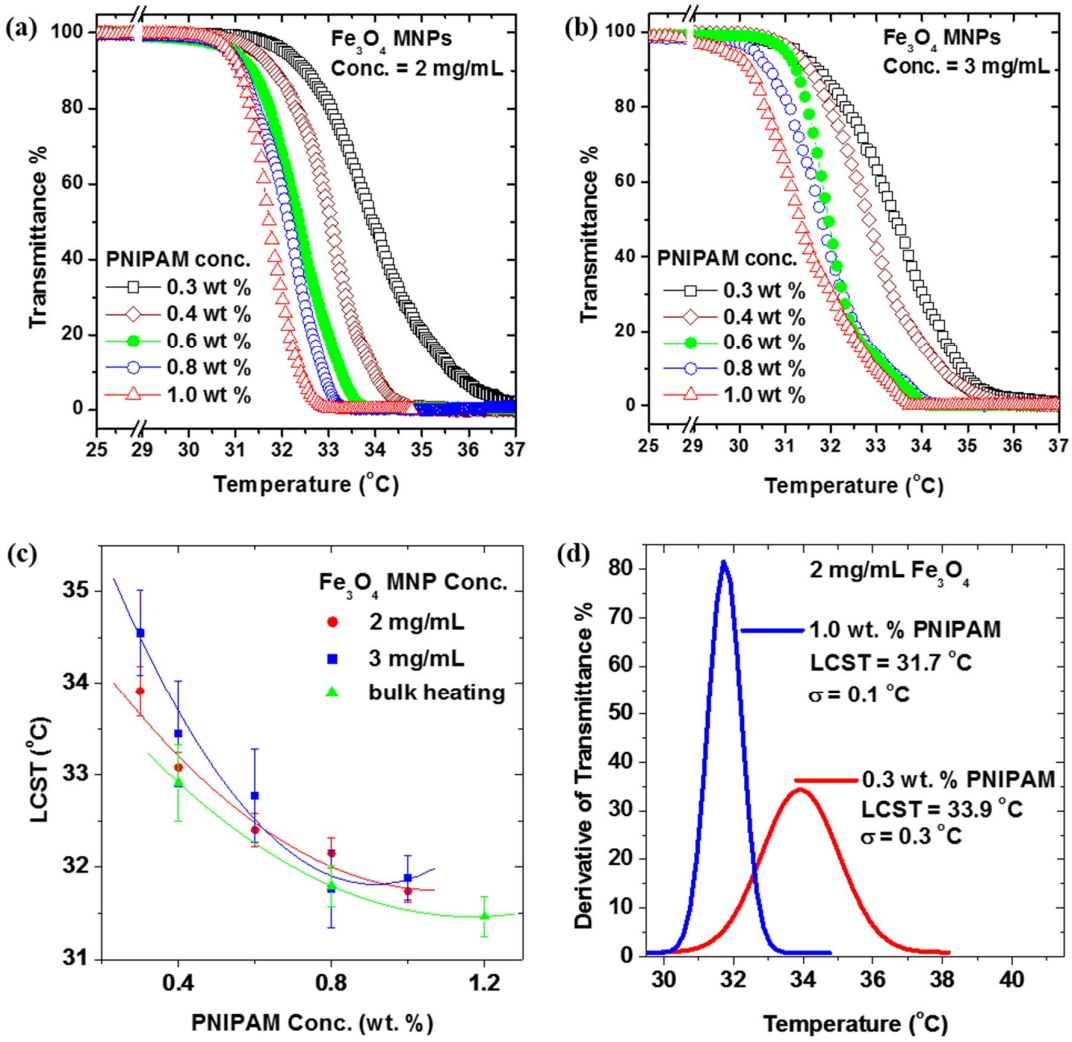

Fig. 5 (a) Aqueous PNIPAM concentration study of transmittance percent as a function of temperature for solutions ranging from 0.3 to 1.0 wt. % polymer content and also containing 2 mg/mL IO MNP content. (b) The same as in (a) only with 3 mg/mL IO MNP content for a relatively faster heating rate of PNIPAM. (c) A comparison of the LCSTs found by relatively slow AMF heating (2 mg/mL IO MNP content), relatively fast AMF heating (3 mg/mL IO MNP content), and bulk heating (non-AMF) as a function of PNIPAM concentration. (d) A comparison of the definiteness of the LCST of a 0.3 wt. % versus a 1.0 wt. % aqueous PNIPAM solution.

% can be changed by tuning the PNIPAM concentration. The LCSTs for PNIPAM/IO MNP aqueous solutions were determined from maxima of the modulus of the derivatives of transmittance percent (see Fig 5(d)). When comparing Figs. 5(a) and 5(b), the change in smoothness of the transmission curves can be attributed to the difference in heating rates. At 2 mg/mL, the heating rate is slower than at 3 mg/mL, as was shown in Fig. 4(a), but the transmittance drop takes place in a more abrupt way. This suggests that in order to get a more defined VPT, the heating rate of the nanoparticles must not be too high, and validates the choice of 2 mg/mL as ideal MNP concentration for the experiments. Considering that the temperature increment necessary for the VPT to take place to be around 10-15 °C (starting at 25 °C), it can be seen that, according to Fig. 4(a), it takes around 150-250 s for the VPT to be completed, depending on the final concentration of MNPs and PNIPAM.

In addition, as shown in Fig. 5(c) a monotonic decrease in the LCST values with increasing PNIPAM concentration is observed for both 2 mg/mL and 3 mg/mL concentrations of IO MNPs. Thus, this suggests that the rate at which PNIPAM samples are heated by AMF does not affect the LCST. The decreasing trend in the LCST of PNIPAM solutions with increasing concentration is consistent with earlier reports on direct heating (i.e. non-RF heating) of PNIPAM solutions [39]. We have further tested this by determining the LCST of PNIPAM solutions heated using a hot bath rather than AMF heating. This

more conventional method of heating PNIPAM yields transition temperatures (green triangles) that are consistent with those of the samples heated with dispersed MNPs that respond to an AMF. This result indicates that the VPT of PNIPAM is not affected by the use of MNPs as a heating source, and therefore confirms them as viable candidates for the remote triggering of the thermal response of the PNIPAM.

The concentration dependent variation in PNIPAM's LCST is a consequence of the fact that critical micelle concentration (CMC) has not been reached. This is demonstrated by Fig. 5(d) in which the derivative of transmittance percent as a function of temperature is given for a 1.0 wt. % versus a 0.3 wt. % PNIPAM/IO MNP solution. Note that the lowest PNIPAM concentrations exhibit a change in state that is poorly defined; it is spread over a wide range of temperature and time. Contrast this with highest PNIPAM concentration in which the phase transformation is more narrow and pronounced; it occurs over a narrow range of temperature and time. As the concentration of the polymer increases, the CMC is approached, beyond which the LCST is constant. Unfortunately, with the experimental setup described above, higher concentrations of PNIPAM could not be investigated. This was due to the fact that for higher concentrations, the samples became opaque to the He-Ne laser making transmittance percent data acquisition impossible.

3.4. Effect of Ions on the LCST of PNIPAM Heated with AMF

Blood is known to contain several different ions in solution to facilitate osmotic balance of blood cells. In order to simulate this aspect of blood, adjusted KOH pellets were dissolved into the initial DIW solvent and then PNIPAM and IO MNPs were added to the solution as described previously. This gave the samples, in the experiments described in this section, a 0.10 M KOH concentration. Figure 6(a) shows the transmittance percent as a function of temperature for PNIPAM concentrations ranging from 0.3 to 1.0 wt. % and a constant IO MNP concentration of 3 mg/mL. As in the previous section, these samples contained PNIPAM in amounts below the CMC and the decrease in LCST with increasing polymer content is the result. However, compared to the 0 M KOH concentration, Fig. 5(b), when we increase the KOH concentration to 0.10 M, both the LCST values and the change in LCST as a function of polymer concentration become smaller. This can be even more clearly seen in Fig. 6(b). In Fig. 6(b), the LCSTs in the presence of OH- ions are compared to those, from the previous section in which ions are not present, at the same 3 mg/mL IO MNP concentration. There is an apparent 2-3 °C decrease in the LCST of PNIPAM/IO MNP solutions at every PNIPAM concentration when the OH^- ions are in solution. This is understood in terms of the "structure maker" influence that OH^- ions have on water molecules. The schematic in Fig. 6(c) depicts how water molecules behave in the presence of OH^- ion and the implications this has on the thermoresponsive polymer. When no ions are present, water molecules are free to randomly orient themselves as in panel (i). In panel (ii), the negative charge of OH^- ions make manifest an electric field that the polar water molecules must align themselves within. For an aqueous PNIPAM solution that contains no OH^- ions the hydration shells, shown in panel (iii), around the hydrophobic acrylic and isopropyl parts of the monomer are relatively swollen since the water molecules are randomly oriented. On the other hand, when the ions are present those same hydration shells, as seen in panel (iv), are relatively shrunken due to the ordered arrangement of water molecules.

There are two ways in which this can be used to explain the reduced LCST [40]. First consider an isopropyl (or acrylic) section of a NIPAM monomer in solution with OH^- ions. Having a smaller hydration shell means less thermal energy is necessary to bring a neighboring isopropyl in proximity. The association of these hydrophobic sections is what ultimately leads to the precipitation of the polymer out of solution. So if this occurs at a reduced thermal energy then the LCST has effectively been reduced. Alternatively, a consideration of the entropy of the system can explain the early onset of LCST. Supposing the hydration shell around the hydrophobic section experiences reduced entropy due to the presence of ions, then the entire system (i.e. the solution) necessarily ends up with increased entropy. This means that the Gibbs free energy of the system becomes entropy dominated earlier as the system heats. Thus the LCST is reduced.

Encouraged by these interesting results, we have also studied how the presence/absence of MNPs affects the LCST. Our MNPs have a negative zeta potential (as usual in this kind of MNP) indicating that their surface is negatively charged. Considering the previous decrease in the LCST obtained when adding OH^- ions to the solution, it is possible that these negative surface charges could also be affecting the LCST. Therefore we have carried out a thorough analysis of the LCST evolution depending on the presence/absence of both MNPs and KOH, using a hot bath as heating source. Interestingly, Fig. 6(b) shows that not only does the presence of KOH effectively reduce the LCST but so does the presence of the IO MNPs. Note that when only PNIPAM is present in solution with DIW the LCSTs brought on by hot bath heating are relatively high (green triangles). Then, when KOH is added to the aqueous PNIPAM there is a small decrease in the LCST at lower concentrations (red triangles). Now when MNPs, but not KOH, are added to the solution there is again a noticeable, yet relatively small, decrease in LCST at all concentrations (pink stars). Finally, when both MNPs and KOH are added to the PNIPAM solutions there is a dramatic lowering of the LCST at every concentration of PNIPAM (black circles).

This indicates that the presence of MNPs inside the PNIPAM is also affecting the LCST and this appears to be related to the presence of negative charges on the surface of our PVP coated nanoparticles. Furthermore, when these residual surface charges on the magnetic nanoparticles interact with the KOH groups, the oleophilic-oleophilic interaction between the isopropyl groups in the PNIPAM accelerate, greatly reducing the transition temperature of PNIPAM.

3.5. Time Lapse Photographs of Samples Correlated to Transmittance and Temperature Data

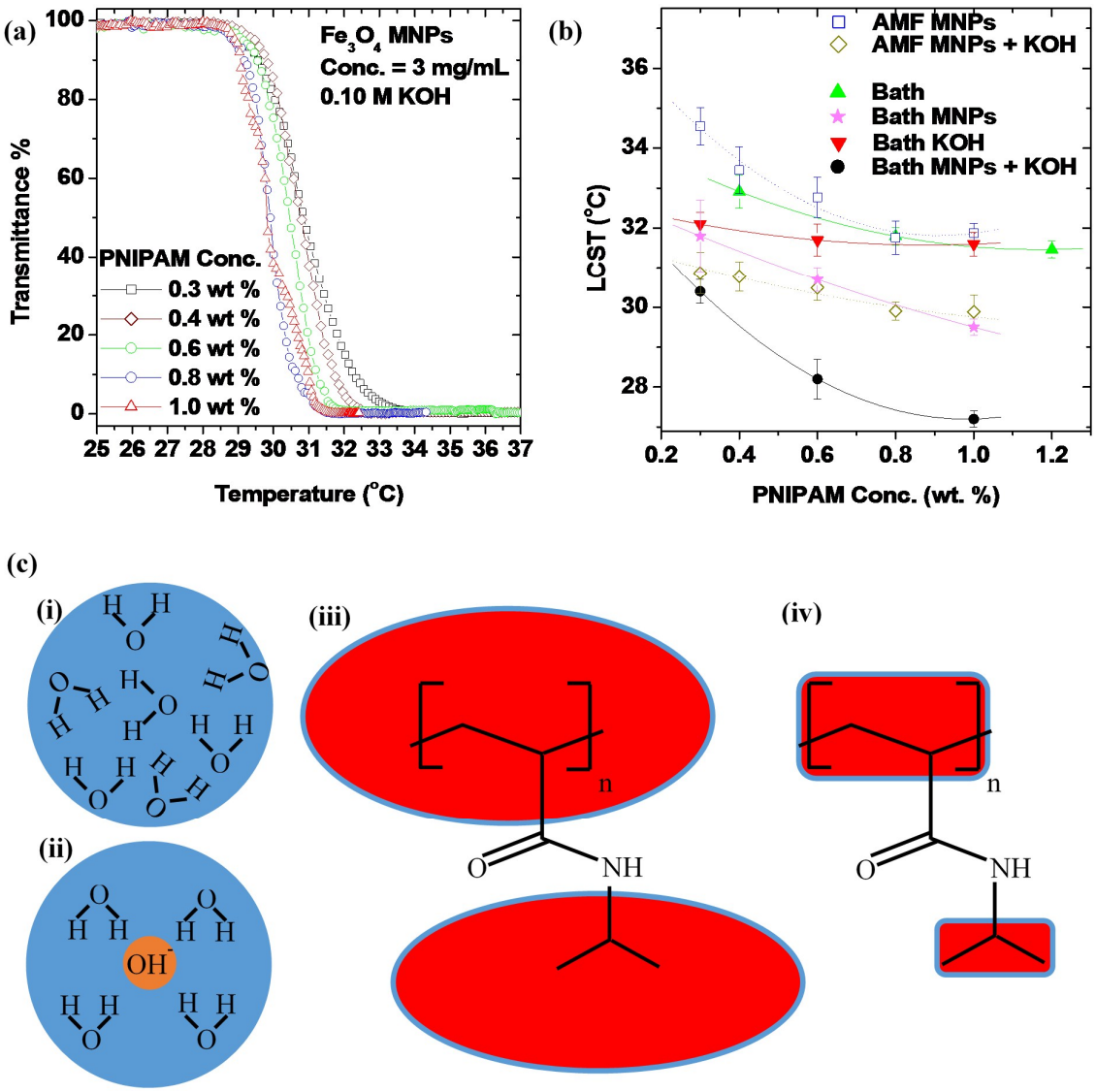

Fig. 6 (a) Aqueous PNIPAM concentration study of transmittance percent as a function of temperature for solutions ranging from 0.3 to 1.0 wt. % polymer content and also containing 2 mg/mL IO MNP content. (b) Study of the effect of IO MNPs and/or KOH on PNIPAM's LCST using either hot bath or RF heating. (c) In panel (i) water molecules orient themselves randomly. In panel (ii) negative charges influence water molecules to take on an ordered orientation. In panel (iii) a NIPAM molecule has swollen hydration shells. In panel (iv) the presence of negative charges in the solution leads to ordered water molecules which in turn leads to shrunken hydration shells.

In order to further demonstrate the phase transformation of aqueous PNIPAM/IO MNP solutions, time lapse photography of the sample was employed and synchronized with both transmittance percent and temperature as a function of time, as shown in Figs. 7(a) and (b) respectively. This was accomplished with an aqueous 0.8 wt. % PNIPAM and 2 mg/mL IO MNP solution. The camera was focused on a logo which was submerged just beneath the surface of the solution. Images from this sample during the trial are shown in Fig. 7(c). For comparison purposes a control sample, containing no PNIPAM and 2 mg/mL IO MNPs, was prepared and its corresponding images are shown in Fig. 7(d).

Note that at the first marked data point (approximately 20 seconds) virtually all of the He-Ne laser passes through the solution. At this same time the sample is approximately 24 °C and the logo appears clear and centered in the frame. This is because the PNIPAM is below its LCST and is in solution with the

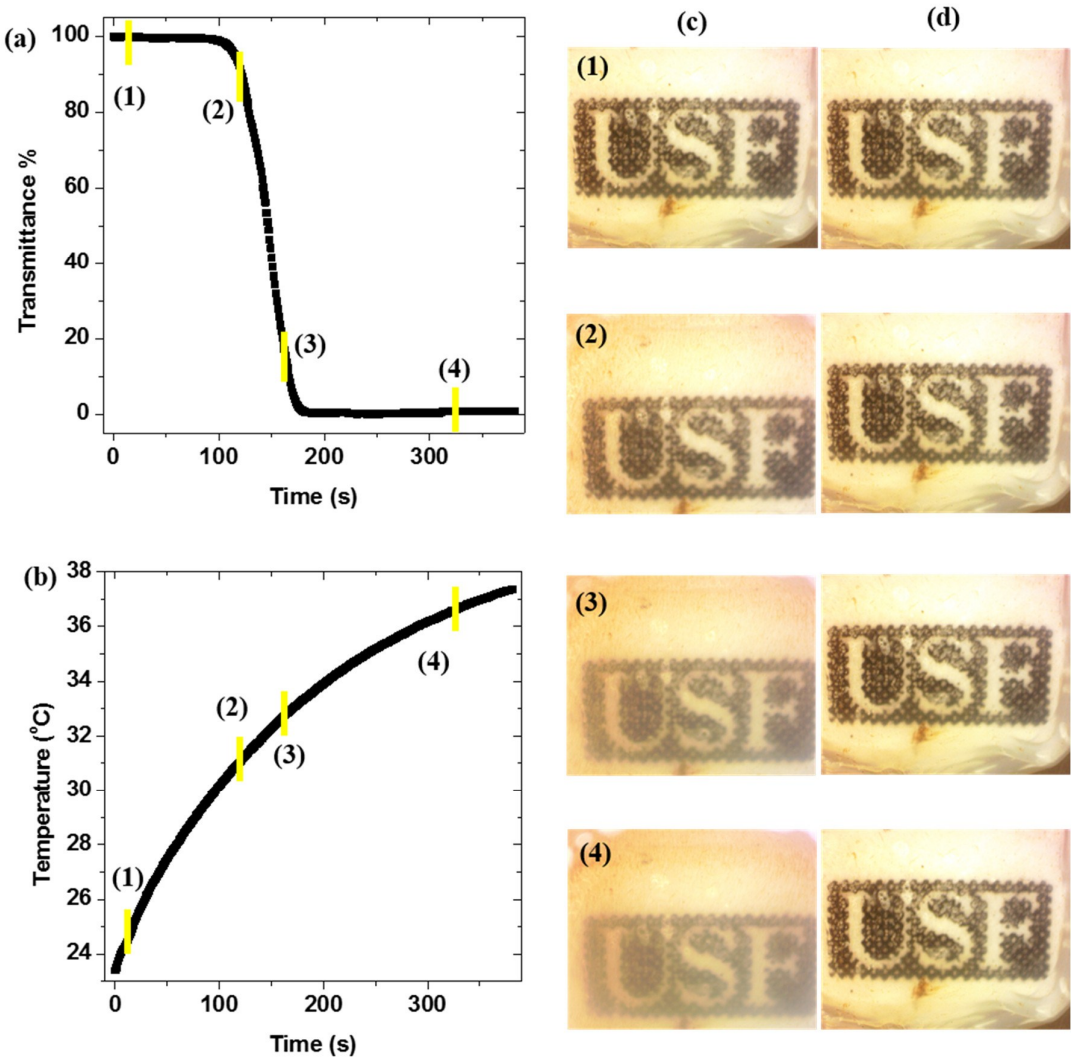

Fig. 7 (a) Transmittance percent versus time of a 0.8 wt. % aqueous PNIPAM solution with 2 mg/mL IO MNPs dispersed therein. (b) Temperature as a function of time of the same solution as it is subject to an AMF. (c) Time lapse photographs of a logo submerged beneath the surface of the solution which was taken at the corresponding marked time in the two data sets. (d) Images of the same logo dispersed in a sample that contained no PNIPAM at the same time intervals.

DIW. Next, at approximately 120 seconds into the trial, the laser has begun to be blocked to around 90 % of its original intensity. This occurs at almost 31 °C (below the LCST) causing the logo to appear slightly hazy and to shift down and to the right in the frame. The image shift is a consequence of the change in refractive index associated with PNIPAM's VPT [41]. The blurring of the logo is due to the increase in the solution's turbidity as the polymer begins to fall out of solution. Then, at nearly 160 seconds, the fraction of He-Ne laser landing on the photodetector is approximately 10 %. At this time the solution is almost 33 °C (above the LCST) which causes the logo to be further obscured. Now most of the polymer has fallen out of solution increasing its turbidity. Finally, at almost 325 s, the laser is fully blocked and the sample has now reached approximately 36 °C (well above the LCST). The logo appears even more turbid than before since now all of the polymer has fallen out of solution. Note that the control solution exhibits no change in turbidity or refractive index since there was no PNIPAM in the solution and so no VPT takes place.

Conclusions

Here a thorough study of the thermal response of linear PNIPAM when heated by IO MNPs in the presence of an AMF was carried out. By comparing the heating rate and SAR curves, the optimal concentration of 10 nm IO MNPs was determined to be around 2 mg/mL. This concentration was shown to provide a smooth VPT in the range of temperatures around 31-

36 °C for the LCST. When increasing the concentration to 3 mg/mL, the LCST is reached faster, but the transition becomes wider and worse defined. In addition, we have shown that the specific point of LCST can be easily tuned by changing the PNIPAM concentration: a monotonic decrease in the LCST values with increasing PNIPAM concentrations is observed for both 2 mg/mL and 3 mg/mL concentrations of IO MNPs, thus suggesting that the rate at which PNIPAM samples are heated by AMF does not affect the LCST. We have also shown, by introducing both OH^- ions and MNPs into the solution the LCST can be made to decrease by 2-3 °C since the hydration shells around the hydrophobic parts of the polymer are reduced in size. Similarly, the addition of MNPs to PNIPAM was shown to decrease the LCST of the polymer due to the negative surface charge which order the surrounding water molecules thus increasing the entropy of the entire system. Finally, time lapse photography was utilized to further demonstrate the VPT of PNIPAM. The work described here provides a more solid foundation for the field of targeted biotherapeutic delivery by exploring the VPT behavior of the stimuli responsive polymer prior to its hybridization with the IO MNP.

Acknowledgements

This work was supported by the United States Army (Grant No. W81XWH1020101/3349). Javier Alonso acknowledges the financial support provided through a postdoctoral fellowship from Basque Government.

References

1 T. Y. Liu, S.H. Hu, D. M. Liu, S. Y. Chen and I. W. Chen, Biomedical nanoparticle carriers with combined thermal and magnetic responses, *Nano Today*, 2009, **4**(1), 52-65.
2 J. O. Martinez, B. S. Brown, N. Quattrocchi, M. Evangelopoulos, M. Ferrari and E. Tasciotti, Multifunctional to multistage delivery systems: The evolution of nanoparticles for biomedical purposes, *Chin. Sci. Bull.*, 2012, **57**(31), 3961-3971.
3 I. Brigger, C. Dupernet and P. Couvreur, Nanoparticles in cancer therapy and diagnosis, *Adv. Drug Deliv. Rev.*, 2002, **54**(5), 631-651.
4 M. Hamidi, A. Azadi and P. Rafiei, Hydrogel nanoparticles in drug delivery, *Adv. Drug Deliv. Rev.*, 2008, **60**(15), 1638-1649.
5 J. Panyam and V. Labhasetwar, Biodegradable nanoparticles for drug and gene delivery to cells and tissue, *Adv. Drug Deliv. Rev.*, 2003, **55**(3), 329-347.
6 S. M. Moghimi, A. C. Hunter and J. C. Murray, Long-circulating and target-specific nanoparticles: theory to practice, *Pharmacol. Rev.*, 2001, **53**(2), 283-318.
7 P. R. Lockman, R. J. Mumper, M. A. Khan and D. D. Allen, Nanoparticle technology for drug delivery across the blood-brain barrier, *Drug Dev. Ind. Pharm.*, 2002, **28**(1), 1-13.
8 K. H. Min, K. Park, Y. S. Kim, S. M. Bae, S. Lee, H. G. Jo, R. W. Park, I. S. Kim, S. Y. Jeong, K. Kim and I. C. Kwon, Hydrophobically modified glycol chitosan nanoparticles-encapsulated camptothecin enhance the drug stability and tumor targeting in cancer therapy, *J. Control Release*, 2008, **127**(3), 208-218.
9 K. Cho, X. Wang, S. Nie, Z. G. Chen and D. M. Shin, Therapeutic nanoparticles for drug delivery in cancer, *Clin. Cancer Res.*, 2008, **14**(5), 1310-1316.
10 A. Ragusa, I. García and S. Penadés, Nanoparticles as nonviral gene delivery vectors, *IEEE Trans. Nanobioscience*, 2007, **6**(4), 319-330.
11 J. D. Kingsley, H. Dou, J. Morehead, B. Rabinow, H. E. Gendelman and C. J. Destache, Nanotechnology: A focus on nanoparticles as a drug delivery system, *J. Neuroimmune Pharmacol.*, 2006, **1**(3), 340-350.
12 M. Nahar, T. Dutta, S. Murugesan, A. Asthana, D. Mishra, V. Rajkumar, M. Tare, S. Saraf and N. K. Jain, Functional polymeric nanoparticles: an efficient and promising tool for active delivery of bioactives, *Crit. Rev. Ther. Drug Carrier Syst.*, 2006, **23**(4), 259-318.
13 Q. A. Pankhurst, J. Connolly, S. K. Jones and J. Dobson, Applications of magnetic nanoparticles in biomedicine, *J. Phys. D: Appl. Phys.*, 2003, **36**(13), R167-R181
14 Q. A. Pankhurst, J. Connolly, S. K. Jones and J. Dobson, Progress in applications of magnetic nanoparticles in biomedicine, *J. Phys. D: Appl. Phys.* 2009, **42**, 224001
15 M. Shibayama and T. Tanaka, Volume phase transition and related phenomena of polymer gels, *Adv. in Polym Sci.*, 1993, **109**, 1-62.
16 D. J. Denmark, D. Mukherjee, J. Bradley, S. Witanachchi and P. Mukherjee, Systematic study on the remote triggering of thermoresponsive hydrogels using RF heating of Fe_3O_4 nanoparticles, Materials Research Society Symposium Proceedings, 2015, 1718, 1718-b04-30.
17 N. A. Peppas, P. Bures, W. Leobandung and H. Ichikawa, Hydrogel in pharmaceutical formulations, *Eur. J. Pharm. Biopharm.*, 2000, **50**(1), 27-46.
18 C. S. Satish, K. P. Satish and H. G. Shivakumar, Hydrogels as controlled drug delivery systems: Synthesis, crosslinking, water and drug transport mechanism, *Indian J. Pharm. Sci.*, 2006, **68**(2), 133-140.
19 F. Ganji and E. Vasheghani-Farahani, Hydrogels in controlled drug delivery systems, *Iran. Polym. J.*, 2009, **18**(1), 63-88.
20 H. G. Schild, Poly(N-isopropylacrylamide): Experiment, theory, and application, *Prog. Polym. Sci.*, 1992, **17**(2), 163-249.
21 F. M. Winnik, Fluorescence studies of aqueous solutions of poly(N-isopropylacrylamide) below and above their LCST, *Macromolecules*, 1990, **23**(1), 233-242.
22 H. G. Schild and D. A. Tirrell, Microcalorimetric detection of lower critical solution temperatures in aqueous polymer solutions, *J. Phys. Chem.*, 1990, **94**(10), 4352-4356.
23 J. Carrey, B. Mehdaoui and M. Respaud, Simple models for dynamic hysteresis loop calculations of magnetic single-domain nanoparticles: Application to magnetic hyperthermia optimization. *Journal of Applied Physics*, 2011, **109**(8), 083921.
24 M. Babincová, V. Altanerová, C. Altaner, P. Cicmanec and P. Babinec, In vivo heating of magnetic nanoparticles in alternating magnetic field, *Medical Physics*, 2004, **31**(8), 2219-2221.
25 A. Jordan, R. Scholz, P. Wust, H. Faehling and R. Felix, Magnetic Fluid Hyperthermia (MFH): Cancer treatment with AC magnetic field induced excitation of biocompatible superparamagnetic nanoparticles, *J. of Magn. and Magn. Mat.*, 1999, **201**(1), 413-419.
26 D. Ortega and Q. Pankhurst, "Magnetic hyperthermia," in Nanoscience: Volume 1: Nanostructures through Chemistry, Cambridge, Royal Society of Chemistry, 60 (2013).
27 C. Binns, "Magnetic Nanoparticle Hyperthermia Treatment of Tumours," in Nanostructured Materials for Magnetoelectronics, Berlin, Springer-Verlag, 197 (2013).

28 A. K. Gupta, and M. Gupta, Synthesis and surface engineering of iron oxide nanoparticles for biomedical applications, *Biomaterials*, 2005, **26**(18), 3995-4021.
29 T. Neuberger, B. Schopf, H. Hofmann, M. Hoffmann and B. von Rechenberg, Superparamagnetic nanoparticles for biomedical applications: possibilities and limitations of a new drug delivery system, *J. Magn. and Magn. Mat.*, 2005, **293**(1), 483-496.
30 M. Mahmoudi, S. Sant, B. Wang, S. Laurent and T. Sen. "Superparamagnetic iron oxide nanoparticles (SPIONs): development, surface modification and applications in chemotherapy." Adv. Drug Deliv. Rev. 2011, **63**(1), 24-46.
31 C. L. Dennis and R. Ivkov, Physics of heat generation using magnetic nanoparticles for hyperthermia, *Int. J. Hyperthermia*, 2013, **29**(8), 715-729.
32 A. Zadrazil, V. Tokarova and F. Stepanek, Remotely triggered release of composite hydrogel sponges, *Soft Matter*, 2012, **8**(6), 1811-1816.
33 J. Cejková, V. Tokárová, A. Pittermannová and F. Stepánek, Remotely controllable microcapsules for site-specific delivery of a chemical payload, http://www.iros2011.org/WorkshopsAndTutorialsProceedings/SW9/iros_11_sw9_17_final.pdf
34 K. Simeonidis, C. Martinez-Boubeta, Ll. Balcells, C. Monty, G. Stavropoulos, M. Mitrakas, A. Matsakidou, G. Vourlias and M. Angelakeris, Fe-based nanoparticles as tunable magnetic particle hyperthermia agents, *J. Appl. Phys.*, 2013, **114**(10), 103904.
35 G. F. Goya, T. S. Berquó, F. C. Fonseca, and M. P. Morales, Static and dynamic magnetic properties of spherical magnetite nanoparticles, *J. Appl. Phys.* 2003, **94**(5), 3520-3528.
36 Z. Ahmed, E. A. Gooding, K. V. Pimenov, L. Wang and S. A. Asher, UV resonance Raman determination of molecular mechanism of poly(N-isopropylacrylamide) volume phase transition, *J. Phys. Chem. B*, 2009, **113**(13), 4248-4256.
37 I. Andreu, E. Natividad, L. Solozábal, O. Roubeau, Nano-objects for Addressing the Control of Nanoparticle Arrangement and Performance in Magnetic Hyperthermia, *ACS Nano*, 2015, **9**, 1408.
38 E. A. Périgo, G. Hemery, O. Sandre, D. Ortega, E. Garaio, F. Plazaola and F. J. Teran Fundamentals and advances in magnetic hyperthermia, *Appl. Phys. Rev*. 2015, **2,** 041302
39 Y. Xia, N. Burke and H. Stover, End group effect on the thermal response of narrow disperse poly(N-isopropylacrylamide) prepared by atom transfer radical polymerization, *Macromolecules*, 2006, **39**(6), 2275-2283.
40 R. Freitag and G. Garret-Flaudy, Salt effects on the thermoprecipitation of poly(N-isopropylacrylamide) oligomers from aqueous solution, *Langmuir*, 2002, **18**(9), 3434-3440.
41 B. W. Garner, T. Cai, S. Ghosh, Z. Hu and A. Neogi, Refractive index change due to volume-phase transition in polyacrylamide gel nanospheres for optoelectronics and bio-photonics, *Appl. Phys. Express*, 2009, **2**(5), 057001.

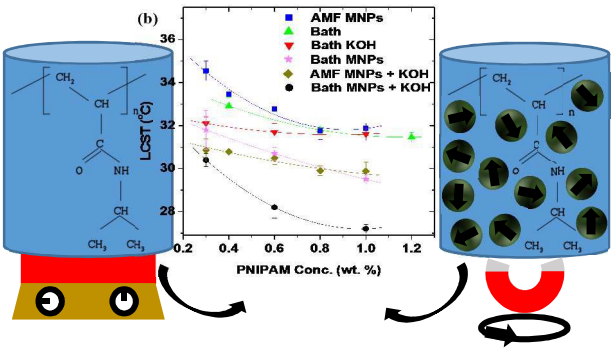

Thermoresponsive PNIPAN can be remotely triggered by embedded iron oxide nanoparticles under an AC field, and the transition temperature can be tuned by changing the ionic